Int. J. Heat Mass Transfer. Vol. 15, pp. 1317–1336. Pergamon Press 1972. Printed in Great Britain

MASS TRANSFER AT ROUGH SURFACES

DAVID A. DAWSON

Hatch Associates Ltd., 21 St. Clair East, Toronto, Ontario, Canada

and

OLEV TRASS

(*Received* 21 *June* 1971)

Abstract—Electrochemical mass transfer rates between solid nickel surfaces and the ferro-ferri-cyanide electrolyte flowing in a 1 in. square duct have been measured for smooth and six similar rough surfaces, the latter having V-shaped grooves of 2–14 mil depth normal to the flow direction. The Reynolds number was varied from 3000 to 120 000, the Schmidt number from 390 to 4600.

For Reynolds numbers greater than about 15 000, these data were correlated as

$$\frac{St_R}{St_S} = \frac{k_R}{k_S} = f(e^+, Sc).$$

A maximum roughness effect was observed at the dimensionless roughness height $e^+ \simeq 10$ where the ratio of rough to smooth surface transfer varied from 3 to 4.

Data for dissimilar surfaces showed the importance of roughness shape and spacing; their influence on mass transfer is different from that on momentum transfer.

NOMENCLATURE

A, cathode area [cm^2];
c, concentration of transferred material [moles/cm^3];
C_f, friction factor $= (2\tau_w g_c/\rho\bar{u}^2)$;
d, diameter [cm];
d_e, equivalent diameter;
$\mathscr{D}$, diffusivity [cm^2/s];
e, roughness height [cm];
e^+, eu^*/ν;
f, friction similarity function, defined by equation (7);
F, fully rough value of f;
$\mathscr{F}$, Faradays' constant 96 500 [A/g equiv. wt];
g, heat transfer similarity function;
g', mass transfer similarity function, defined by equation (12);
g'', St_R/St_S;
g_c, gravitational constant 980 [g cm/g$_f$ s^2];
I, cell current [A];
I_{lim}, limiting cell current [A];
K, mass transfer coefficient [cm/s];
K^+, $[St/\sqrt{(C_f/2)}]$;
l, width of duct wall [cm];
p, roughness spacing [cm];
Pr, Prandtl number;
Re, Reynolds number $= d_e\bar{u}/\nu$;
s, distance between pressure taps [cm];
Sc, Schmidt number $= \nu/\mathscr{D}$;
Sh, Sherwood number $= kd_e/\mathscr{D}$;
St, Stanton number $= Sh/Re\,Sc$;
u, velocity in downstream direction [cm/s];
$\bar{u}$, mean velocity [cm/s];
u^*, "friction velocity" $= \sqrt{(\tau_w g_c/\rho)}$ [cm/s];
V, applied voltage [V];
y, distance normal to duct wall [cm];
y^+, yu^*/ν;
Z, valence change [equiv. wt/mole].

Greek letters

ΔP, pressure drop [g$_f$/cm^2];
ε, eddy viscosity [cm^2/s];

ε_D, eddy diffusivity [cm^2/s];
μ, viscosity [g/cm s];
ν, kinematic viscosity $= \mu/\rho$ [cm^2/s];
ρ, density [g/cm^2];
τ, shear stress [g_f/cm^2].

Subscripts
B, bulk or average;
R, rough surface;
S, smooth surface;
W, wall.

ALTHOUGH the processes of momentum, heat and mass transfer near a smooth surface are reasonably well understood, the effect of surface roughness on the transfer rates is not. Theoretical analysis of flow near a rough surface is at best qualitative, while empirical correlation of the transfer rates is hampered by the inability to find suitable parameters to describe the roughness.

Surfaces with roughness elements entirely within the viscous sublayer have been found to be 'hydraulically smooth' [1]; heat transfer coefficients for such surfaces have also shown no roughness effect [2]. Brennan [3] has suggested, however, that in high Schmidt number mass transfer systems, where the resistance to transfer is concentrated within the viscous sublayer, even very small roughnesses could significantly increase the transfer rate. A fourfold range exists in the mass transfer data available in the literature, as shown in Fig. 1, which Brennan attributes to the formation of minute roughnesses on the surfaces as they dissolve.

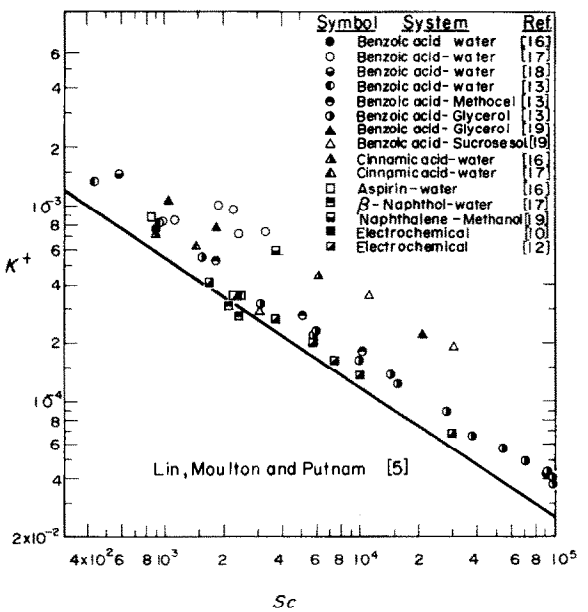

FIG. 1. Smooth surface mass transfer at high Schmidt number. Literature data.

Larger surface roughnesses, at high velocities, affect the three transfer processes differently—the friction factor becomes constant at high Reynolds numbers [1], while heat and mass transfer coefficients continue to depend on fluid properties [2, 4]. It is questionable whether the three transfer processes can be considered analogous under these conditions, except in a microscopic sense.

In the present study, mass transfer rates have been measured over a range of variables which includes the areas discussed above. The electrochemical technique employed is particularly suited to roughness studies, since the surface does not dissolve during the transfer process. Thus, in contrast to the dissolution techniques, the surface geometry can be predetermined, and will remain constant.

THE ELECTROCHEMICAL TECHNIQUE

Until recently, most mass transfer studies were performed by measuring the rate of thickness decrease of a surface dissolving in a fluid. In the last decade, the electrochemical technique of mass transfer measurement has become popular, partially because of its capability for rapid, precise measurement of transfer rates, but particularly because the transfer process causes no change in the surface.

The basic principles of the technique will not be discussed in any detail here, as these have been adequately described elsewhere [5–10]. Essentially, the method involves the measurement of the current flowing in an electrochemical cell,

operating under such conditions that the reaction rate is controlled by the diffusion toward the electrode surface of a particular ion of known concentration.

In this study, the cell consisted of two nickel electrodes, on opposite walls of a one-in. square duct, through which flowed an electrolyte solution. The electrolyte composition was typically

$K_3Fe(CN)_6$	$3{\cdot}5 \times 10^{-3}$M
$K_4Fe(CN)_6$	$7{\cdot}0 \times 10^{-3}$M
NaOH	1–4M

When a voltage is applied to the cell, the reaction

$$Fe(CN)_6^{-3} + e^- \rightarrow Fe(CN)_6^{-4}$$

occurs at the cathode, and the reverse reaction at the anode. The surface to be studied was made the cathode of the cell; a smooth electrode of approximately three times the surface area was used as the anode. Since the cathode was smaller, and the ferricyanide ion concentration was less than that of ferrocyanide, the processes occurring at the cathode controlled the cell current. This was tested experimentally by varying the concentration of ferrocyanide ion; no change in the cell current was observed, using rough or smooth cathodes.

In systems such as this in which the mass transfer rates are high, proper preparation of the electrode surface is necessary to ensure that the surface reaction rate will not be the controlling factor. Hanratty and co-workers [7–10] have shown that a satisfactory cleaning procedure consisted of buffing the surface, followed by cathodic treatment in an electrolysis cell. In the present study, a similar method of surface preparation was found inadequate for the rough electrodes, likely because of the etched structure of the surfaces. After some experimentation, it was found that rinsing the surface for a few seconds with dilute (1N) sulphuric acid solution after buffing with a commercial cleanser, followed by 30 min cathodic treatment in a 1N sodium hydroxide electrolysis cell, resulted in

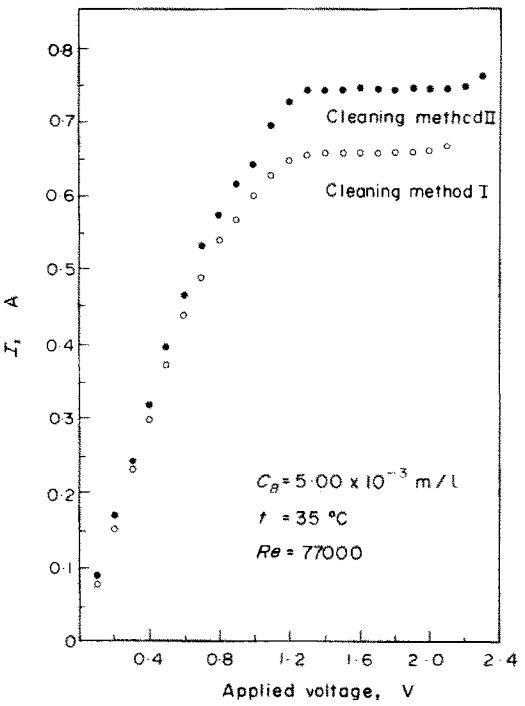

FIG. 2. Polarization curves for surface R3, cleaning methods I and II.

good, reproducible polarization curves. A complete description of the method of surface preparation may be found in [11].

It is normally assumed in electrochemical mass transfer studies that a flat plateau in the polarization curve is adequate proof of diffusion control. The data in Fig. 2 demonstrate that this is not necessarily the case. These polarization curves were obtained using two different methods of cleaning the surface, but under otherwise identical conditions; although both curves have excellent plateaux, the limiting currents differ by 15 per cent. These results cast some doubt on the validity of the technique, and on published data obtained by this method.

A further test is required to ensure that the cell is truly diffusion controlled. The dependence of the limiting current on ferricyanide ion concentration should be linear under diffusion control, while under the combined influence of

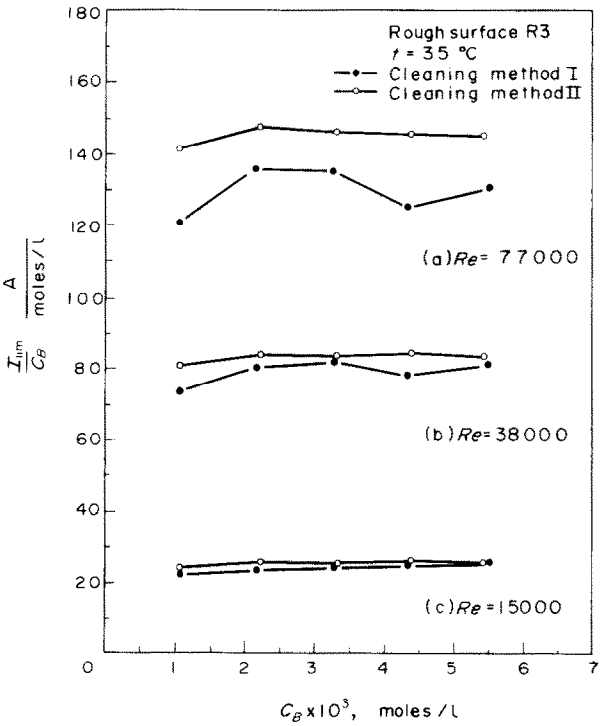

FIG. 3. The effect of concentration on the limiting current.

diffusion and surface reaction, such a linear relationship would not be expected. The results of this test are illustrated in Fig. 3. Using the cleaning procedure described above, denoted Cleaning Method II, the ratio I_{lim}/C_B is independent of C_B. The results for Cleaning Method I show no definite trend away from linearity, but are badly scattered, especially at the highest Reynolds number. If the surface reaction rate is affecting the limiting current, its influence would of course be strongest at high Reynolds numbers, where the diffusion rate is greatest.

EXPERIMENTAL

Rough surface electrodes

Of the eight rough surfaces for which mass transfer and friction factor data are reported, six (R1-R6) belonged to a geometrically similar series. The roughness elements were V-shaped grooves running across the flow direction. Within the limits of the method of fabrication, the ratio of groove pitch to height was held constant.

To fabricate these surfaces, a pattern was first drawn consisting of a series of parallel lines 4 units thick and 50 units apart. From this drawing, six photographic negatives were made using a different degree of reduction for each. The patterns were then photoengraved onto $\frac{1}{16}$th in. nickel plates, the depth of the etch being controlled as much as possible to be proportional to the line spacing. The resulting groove dimensions were as given in Table 1;

Table 1. Roughness dimensions

Surface	Pitch, p (mils)	Height, e (mils)	p/e
R1	10	2·2	4·5
R2	15	4·0	3·75
R3	20	5·2	3·75
R4	30	8·0	3·75
R5	40	11·0	3·64
R6	50	13·6	3·68
R7	15	4·1	3·66
R8	30	4·0	7·5

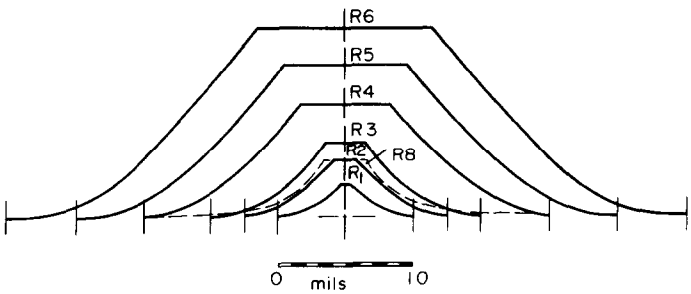

FIG. 4. Sketch to scale of the roughness elements.

except for surface R1, which had a slightly shallow groove, the p/e ratios for the six surfaces were quite consistent.

Figure 4 shows a sketch of each of the surfaces, drawn to scale, to illustrate the relative sizes and shapes of the roughness elements. The flat top of each of the roughnesses was the original, unetched surface of the nickel plate, while the curved surface was the etched groove. The groove surface was of course not perfectly smooth as shown here, but exhibited a graininess of about 0·2 mils in height resulting from the etching process.

The other two rough surfaces, R7 and R8, had different geometrical configurations. These were not studied in any detail, however, and were intended only as a comparison to aid in the understanding of the results from the six similar surfaces.

Surface R7 was made from a different pattern drawing; instead of continuous parallel lines as for the other six surfaces, the pattern consisted of a series of dashes 50 units long, separated by 50 unit spaces. Alternate lines were staggered such that the dashes were opposite the spaces of the adjacent lines. The pattern was reduced to the same dimensions as surface R2, and the etch depth was the same as R2. The result was a surface on which the roughness elements were broken to provide a flow path around the elements.

Surface R8 was made using the pattern for surface R4 of the similar series, but was etched to the same depth as surface R2. R8 therefore had twice the p/e ratio of the similar series of roughnesses, and was designed to illustrate the effect of this ratio on the transfer rates.

The plates were cut after etching to a size of 12 in. long by $\frac{3}{4}$ in. wide. Brass screws were soldered to the back of the plates for use as mounting bolts and electrical connectors.

Mass transfer experiments

An overall schematic diagram of the experimental flow system is given in Fig. 5. The system formed a closed loop from the pump through the entrance and test sections, the rotameter, and a 15 gallon polyethylene surge tank. A bypass loop was provided to allow better control of the flow rate. All components of the system, with the exception of the stainless steel cooling coil, were non-metallic, to avoid contamination of the system by corrosion. Nitrogen required to deoxygenate the solution prior to the start of an experiment was supplied to the pump inlet by a glass tube inserted through the top of the surge tank. The tank was covered to keep a blanket of nitrogen over the solution, and was wrapped with aluminium foil to exclude light.

The one-in. square Lucite test section was 24 in. long, and was preceded in the flow loop by a 36 in. long entrance section of the same internal dimensions, to ensure a fully developed velocity profile.

The lower wall of the test section was grooved to receive a smooth nickel anode covering the width of the duct for the entire length of 24 in. A 12 in. × 1 in. slot was cut in the upper wall, into which fitted a removable cover plate con-

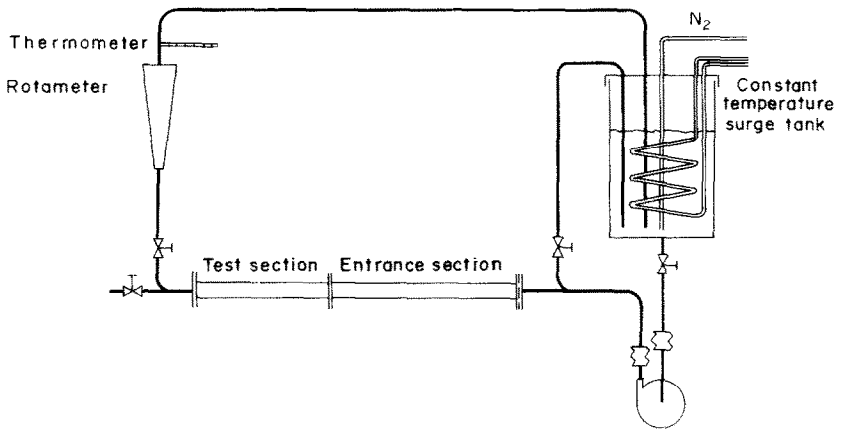

FIG. 5. Schematic diagram of electrolyte flow system.

taining the cathode. A cross-sectional view of the duct is given in Fig. 6, showing the cover plate clamped in place, and sealed with an O-ring.

A $\frac{1}{16}$th in. deep slot was machined into the face of the cover plate to hold the cathode, and three holes were drilled through the plate to accommodate the cathode bolts. When the complete test section was assembled, the peaks of the roughness were flush with the duct wall.

A simple electrical circuit supplied power to the electrolytic cell. A 6-V lead–acid battery was used as the power source; the voltage applied to the cell was controlled with a 25 Ω, ten-turn helical potentiometer and measured on a small voltmeter. The cell current was indicated on a 1 A Weston D.C. ammeter; the voltage drop across the ammeter, previously calibrated, was recorded on a Leeds–Northrup AZAR mV recorder, having an adjustable range from 0·67 to 100 mV, and an adjustable zero from −50 mV to +50 mV.

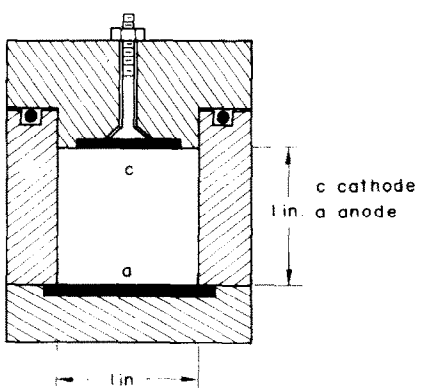

FIG. 6. Cross-section of test section.

The electrolyte solution was prepared in the equipment, by adding weighed amounts of sodium hydroxide, potassium ferricyanide and potassium ferrocyanide to approximately 40 l. of distilled water in the surge tank. The solution was pumped around the loop to ensure thorough mixing. Sodium hydroxide concentration was tested by titrating a sample with 1N HCl, and adjusted if required. The ferricyanide concentration was titrated iodometrically either just before or just after a run was performed, using starch solution as an indicator.

To begin a mass transfer experiment, the required cathode was inserted in the cover plate and cleaned using Method II described above. At the same time, a dummy cover plate was installed in the test section, and the solution circulated. The electrolyte was brought up to the required temperature, and held there by circulating cooling water from a constant temperature bath through the coil. The temperature was controlled to within 0·5°C by this method. During the first half of the 30 min warmup period,

nitrogen was introduced to the pump inlet to purge the solution of oxygen.

The clean electrode was installed in the test section, and connected into the electrical circuit. A polarization curve was measured in steps of 0·1 V at the highest flow rate. Limiting current measurements were then taken over the whole range of flow rates, beginning with the highest. Although polarization curves were not taken at each flow rate, the voltage was reset for each reading after a quick scan of the plateau. After all readings had been taken, the first measurement was rechecked to give an indication of drift caused by contamination. The drift over the roughly 30 min duration of the run was rarely more than 3 per cent; if the drift exceeded 5 per cent, the data were discarded and a new solution prepared. Since the drift only affected the high flow rate readings, which were taken during the first few minutes of the run, it is estimated that no reading would be more than 1 per cent below its initial value.

Mass transfer coefficients were calculated from the limiting current using the equation

$$K = \frac{I_{\lim}}{Z\mathcal{F}AC_B}. \tag{1}$$

Friction factor measurements

An initial attempt to measure friction factors in the mass transfer flow loop failed, as the pressure drops over the short test section were too small for accurate measurement. A Decker model 306 differential pressure meter was available, however, which was capable of measuring pressure differences of 10^{-3} in. of water, in a gas. The meter was equipped with two interchangeable transducers having nominal ranges of 0·1 and 3·0 in. of water. The output of the meter, 0–10 V d.c., was stepped down to 0–50 mV with a resistance bridge, and was recorded on the AZAR recorder. The meter system was calibrated against an inclined manometer prior to use.

The same one-in. square duct from the mass transfer experiments was used for the measurement of pressure drops in air. Air was supplied by a rotary positive displacement blower, through a surge tank and rotameter, to the square duct. So that the rough and smooth surfaces could be compared at exactly the same flow rate, two identical test sections were installed after the 36 in. long entrance section. Pressure taps were located 2 in. downstream from the leading edge, and one in. upstream from the trailing edge, of the 12 in. long surface in each section. Either set of taps could be connected to the meter using three-way stopcocks. As the rough surface did not extend over the whole perimeter of the duct, the friction factor could not be calculated directly from the pressure drop measurement. If it is assumed, however, that the rough surface contributes to the pressure drop in proportion to the fraction of the surface area which it occupies, then the rough surface friction factor can be calculated from the increase in pressure drop caused by the rough surface over the equivalent value for the smooth surface. A momentum balance over a length, s, of the square duct, part of whose surface, A, is roughened, yields

$$\Delta P_R \cdot l^2 = \tau_{WR} \cdot A + \tau_{WS} \cdot (4ls - A). \tag{2}$$

When the surface is smooth, this reduces to

$$\Delta P_s \cdot l^2 = \tau_{WS} \cdot (4ls). \tag{3}$$

Using the definition of the friction factor, C_f, these equations can be combined to give

$$\frac{C_{fR}}{C_{fs}} = 1 + \frac{4ls}{A}\left(\frac{\Delta P_R - \Delta P_S}{\Delta P_S}\right). \tag{4}$$

RESULTS

Friction factor data

Friction factors measured for the smooth-walled duct, and for the geometrically similar series of rough surfaces, are plotted in Fig. 7. The results cover a Reynolds number range from 10000, considered to be the lowest flow rate at which meaningful pressure drops could be measured, to about 60000.

The smooth surface data follow an approximately linear plot, with a small negative slope,

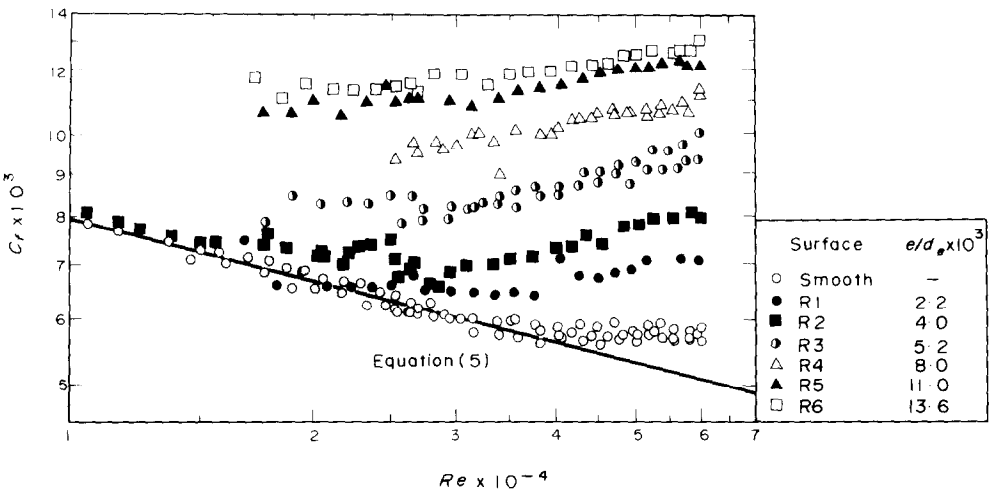

FIG. 7. Uncorrected friction factor data, surfaces R1–R6.

and except at high Reynolds numbers are in good agreement with the well-known Blasius equation for smooth round tubes.

$$C_f = 0{\cdot}0791\, Re^{-\frac{1}{4}}. \qquad (5)$$

A gradual positive deviation from the Blasius line can be observed as the Reynolds number is increased. It was attributed to imperfections in the duct construction and in the fitting of the cover plate.

The data for the rough surfaces were calculated from the difference between the rough and smooth pressure drops, and as a result are considerably scattered. The data are of sufficient accuracy, however, to illustrate trends with Reynolds number and roughness height. In the range of Re studied, no single surface covers the full friction factor range from hydraulically smooth to fully rough. However, by examining the data for successively larger roughnesses, the whole range can be observed.

At low Re, for the smallest roughnesses, the friction factor curve coincides with that for the smooth surface. With increasing Reynolds

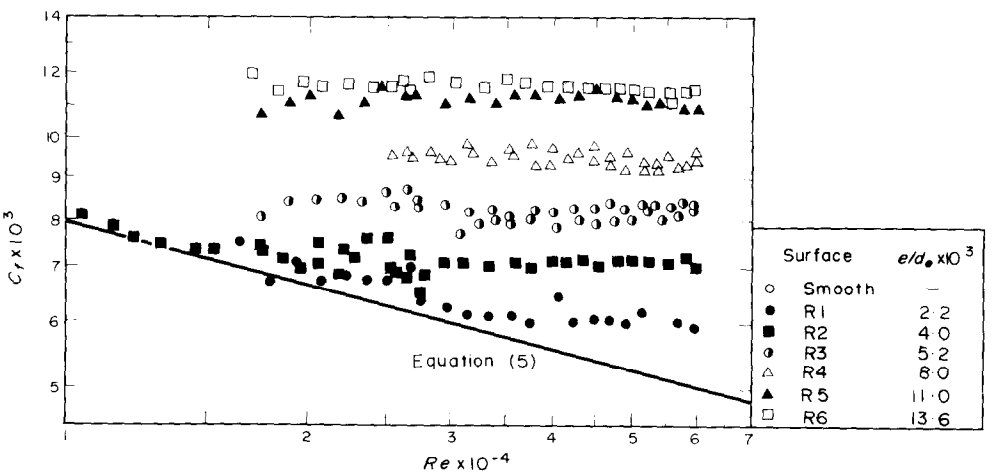

FIG. 8. Corrected friction factor data, surfaces R1–R6.

number and roughness height, the friction factor rises from the smooth curve. The data do not level out to a horizontal line, as would be expected from previous work [1], but continue to rise with increasing Re.

Since C_{f_R} is calculated as a multiple of C_{f_s} at the same Reynolds number, the error observed in the smooth surface results is of course carried over to the rough surface friction factors as well. This error can be eliminated from C_{f_R} by correcting the equivalent value of C_{f_s} to coincide with the Blasius line.

The rough surface friction factors have been replotted in the corrected form in Fig. 8. The results for each of the six similar surfaces now level out to a constant value at high Reynolds numbers, this value increasing with increasing roughness height. The fact that this correction yields a result consistent with previous work [1, 4] gives some degree of confidence in the validity of the measured ratio C_{f_R}/C_{f_s}, although there are errors in the smooth surface data at high Re.

Figure 9 is a similar plot of the friction factor data for surfaces R2, R7 and R8, corrected as above for errors in C_{f_s}. These results show the effect of the shape of the roughness on the friction factor; although each of these surfaces has the same roughness height, the friction factors differ markedly. Obviously, the pitch/height ratio, p/e, and the roughness pattern have an important effect on the friction factor; we shall see below that the mass transfer coefficients are also affected.

Mass transfer coefficients

Using the electrochemical technique described above, mass transfer coefficients in the range $3000 \leqslant Re \leqslant 120000$ have been measured at ten different values of the Schmidt number from 400 to 4600. The data plotted in Figs. 10–12 are typical; a complete tabulation of all the results can be found in [11].

As expected, the smooth surface data form straight lines on the logarithmic plots of the Sherwood number against the Reynolds number, with slopes just less than one. These lines shift progressively higher as the Schmidt number is increased, indicating a positive exponent on Sc. Correlation of the smooth surface data, using a least-squares analysis, yielded the equation

$$Sh = 0{\cdot}0153\, Re^{0{\cdot}88}\, Sc^{0{\cdot}32} \qquad (6)$$

with a standard deviation of 4 per cent.

The exponents on Re and Sh are in excellent agreement with the values predicted by Lin *et al.* [5] of $\frac{7}{8}$ and $\frac{1}{3}$ respectively. The data average 32 per cent higher than Lin's equation, however. By comparison, Hubbard [12] and Son and Hanratty [10] each reported data averaging 11 per cent above Lin's prediction. The data of Harriot and Hamilton [13] for dissolution mass transfer are about 25 per cent higher.

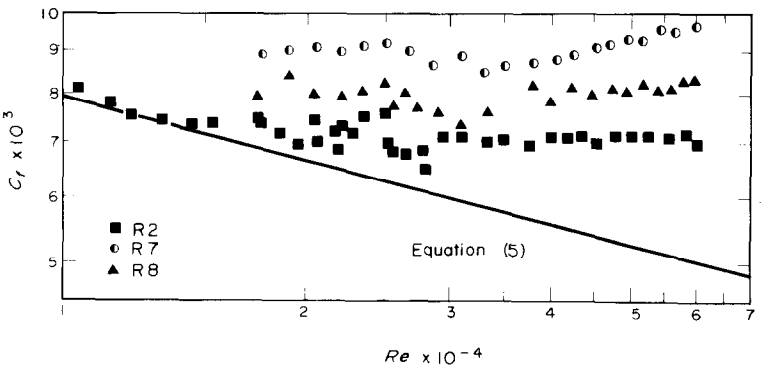

FIG. 9. Corrected friction factor data, surfaces R2, R7 and R8.

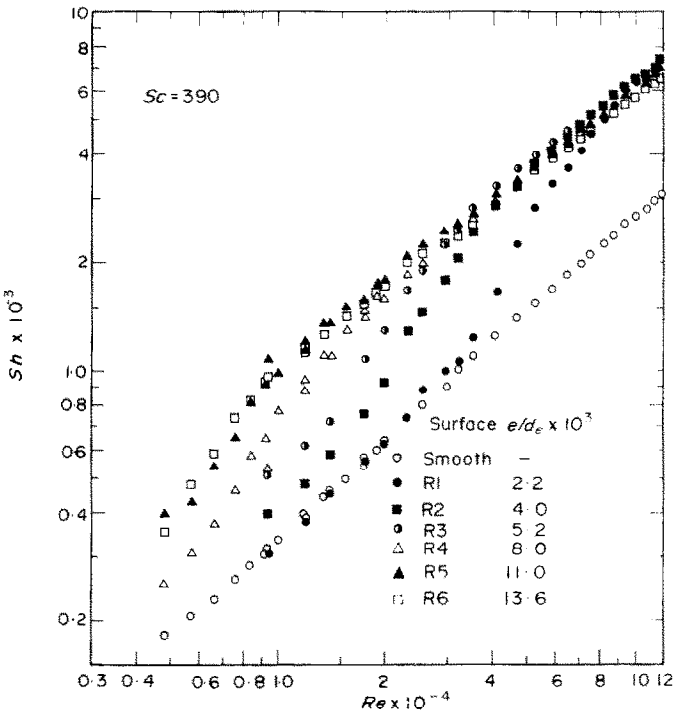

FIG. 10. Dimensionless mass transfer coefficients, surfaces R1–R6, Sc = 390.

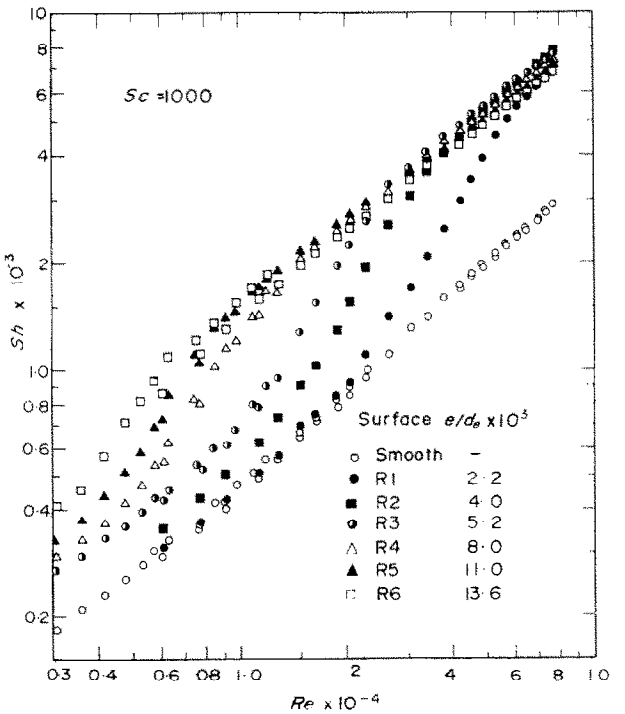

FIG. 11. Dimensionless mass transfer coefficients, surfaces R1–R6, Sc = 1000.

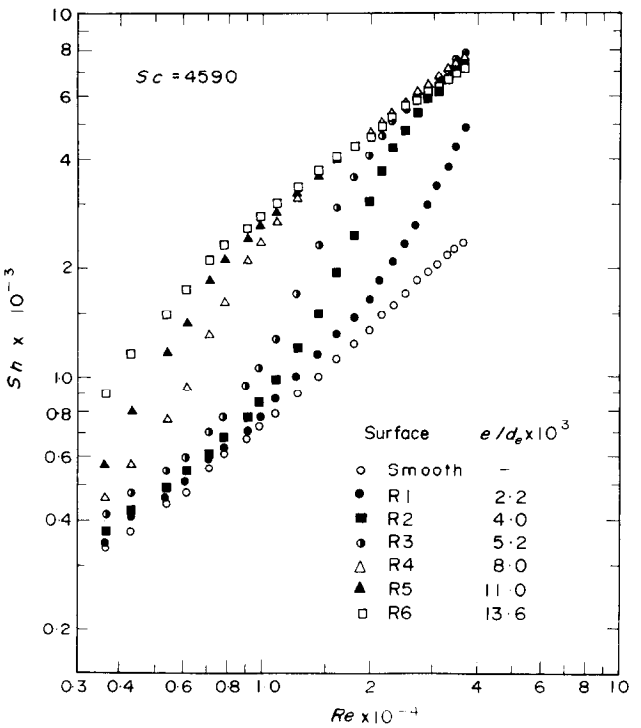

FIG. 12. Dimensionless mass transfer coefficients, surfaces R1–R6, $Sc = 4590$.

The present data, then, appear to be slighly above the available literature values. This discrepancy is believed to result from entrance effects, since no mass transfer entry length was provided, and from edge effects at the sides of the electrodes, resulting from bulk circulation of the fluid in the square duct. The error introduced by these effects was estimated [11] at 26 per cent at $Re = 3000$, but dropping rapidly to less than 5 per cent above $Re = 25000$. It is expected that similar errors would occur in the rough surface data; thus the use of the ratio of rough to smooth surface coefficients to correlate the data should result in a partial cancellation of errors.

The rough surface results follow a quite different trend with Re from those for the smooth surface. At low Re, the data form a series of lines parallel to the smooth surface line. The data for the surface with the smallest roughness, R1, coincide with those for the smooth surface, at all Sc. The lines for the other rough surfaces are progressively higher for increasing roughness heights.

As the Reynolds number is increased, the rough surface curves begin to deviate from the linear relationship between log Sh and log Re, and undergo a rapid increase over a narrow range of Re. The Reynolds number at which this transition begins depends on the roughness height of the surface; at $Sc = 1000$ for example, R1 begins transition at about $Re = 20000$, while for R5 this occurs at $Re = 4000$. The roughest surface, R6, is in the transition region at the lowest Re recorded, 3000. A comparison of the curves for different Schmidt numbers shows these values to be slightly lower at high Sc.

At still higher Reynolds numbers the influence of the surface roughness reaches a maximum, beyond which the curves level off into a second linear region having a slightly lower slope than the smooth line. This maximum also occurs at progressively lower Reynolds numbers as the roughness height is increased. The maximum

improvement in mass transfer shows very little dependence on the roughness height, but varies considerably with Sc. A maximum factor of three improvement is obtained at $Sc = 390$, while at $Sc = 4590$ this ratio is approximately four.

Because the improvement in the transfer rate decreases from this maximum, a rather surprising result occurs at high Re—greater transfer rates are obtained with the smaller roughnesses. This is quite contradictory to what one would predict intuitively. It is apparent from this result that the use of the friction factor to specify the roughness is quite inadequate. It is also difficult to defend the use of the "equivalent sand roughness" as a correlating variable for rough surface heat and mass transfer rates, since it is simply a redefined friction factor.

Further evidence that the friction factor is an insufficient description of the roughness can be found in the results for the three dissimilar surfaces R2, R7 and R8, which have the same roughness height. A representative set of these is shown in Fig. 13. All three surfaces yield essentially identical curves in the low Reynolds number and transition regions. At high Reynolds numbers the curves separate slightly; surface R2 gives the highest transfer rate, while the data for R7 and R8 are about 5 and 15 per cent lower, respectively. The friction factors for these surfaces, as shown previously in Fig. 9, show an entirely different trend. R2 has the lowest friction factor, while the value for R7 is about 30 per cent higher, and that for R8 about 15 per cent higher than R2. It is obviously impossible to correlate the mass transfer data on the basis of friction factor alone: one or more additional parameters are necessary to express the effect of roughness shape.

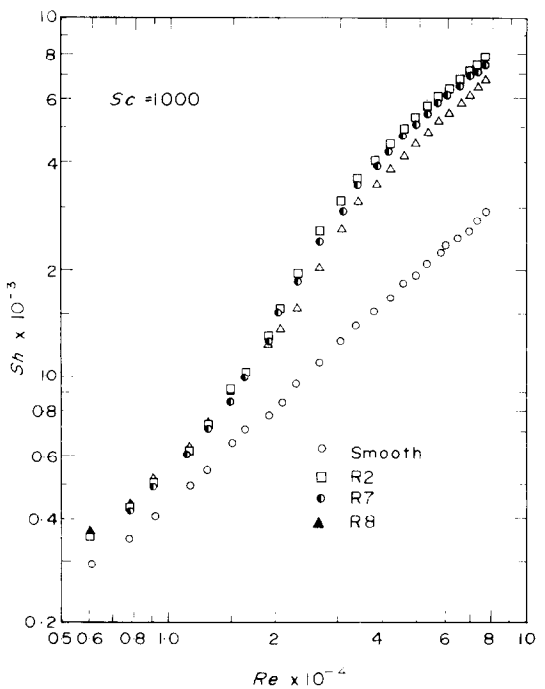

FIG. 13. Dimensionless mass transfer coefficients, surfaces R2, R7 and R8.

DISCUSSION OF RESULTS

In order to correlate the mass transfer coefficients for the series of similar roughnesses, a similarity analysis has been performed following the procedure of Dipprey and Sabersky [2] for heat transfer.

Friction similarity functions

Before an analysis of the rough surface mass transfer data is attempted, it is necessary to ensure that the friction similarity concept holds for this type of roughness. Nikuradse [1] derived the following expression for the friction similarity function

$$f(e^+) = \sqrt{\left(\frac{2}{C_f}\right)} + 2{\cdot}5 \ln \frac{2e}{d} + 3{\cdot}75 \qquad (7)$$

and found that this function correlated his friction factor data for a series of sand-roughened tubes. The corrected friction factor data of the present work are plotted in the same form in Fig. 14, along with Nikuradse's curve. Although the data points are quite scattered, it is apparent that this method of correlation reduces the results

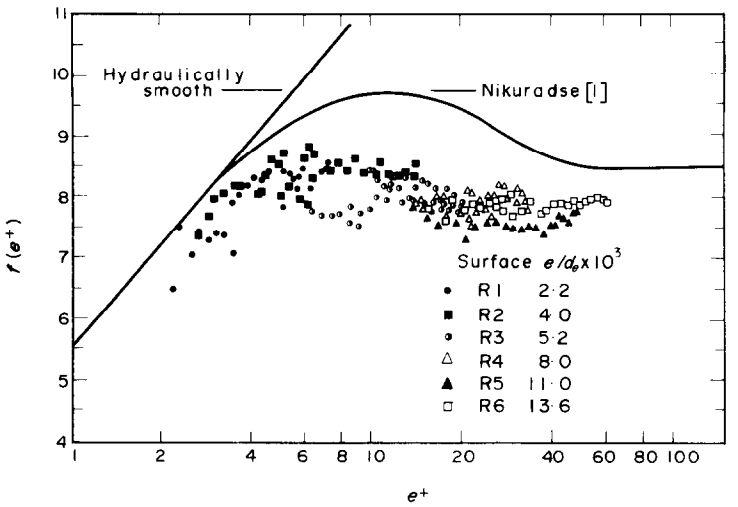

FIG. 14. Friction similarity function, surfaces R1–R6.

to a single curve. There are discrepancies between the results for each surface, but no trend with e/d_e is evident. The shape of the resulting curve is similar to that of Nikuradse, approaching the hydraulically smooth line at low e^+, and levelling out to a constant value at high e^+. The maximum in the transition region is much less prominent than that obtained by Nikuradse, indicating a more gradual transition of the friction factor to its fully rough value.

Just as the Blasius equation, (5), is an approximation of Prandtl's more theoretically correct logarithmic expression, Nikuradse's expression for the fully rough friction factor can also be approximated by an exponential function.

$$C_{f_R} = \text{const}\left(\frac{e}{d}\right)^{\frac{1}{4}}. \tag{8}$$

Combining equations (5) and (8), one would expect the ratio C_{f_R}/C_{f_s} to vary as $e^{+\frac{1}{4}}$ in the fully rough region, with the hope that e^+ will adequately correlate the ratio in the hydraulically smooth and transition regions as well.

Such a plot is shown in Fig. 15. A good correlation of the data is obtained, considering the scatter in the original measurements. The ratio C_{f_R}/C_{f_s} has a value of unity for $e^+ \leqslant 3$, and can be reasonably well described in the range $e^+ > 3$ by

$$\frac{C_{f_R}}{C_{f_s}} = 0{\cdot}675\, e^{+0{\cdot}30}. \tag{9}$$

The expected slope of $\frac{1}{4}$ is not obtained, probably because the data do not extend far enough into the fully rough region. The correlation, however, gives a reasonable basis on which to conclude that the geometrically similar series of roughnesses does exhibit friction similarly as well.

The mass transfer similarity hypothesis

Following the procedure outlined by Dipprey and Sabersky [2] for heat transfer, the mass transfer similarity function can be derived. The derivation is identical to that of Sherwood [14] for smooth surfaces, and results in the same equation.

$$\frac{(C_f/2\,St) - 1}{\sqrt{(C_f/2)}} = \int_0^{y_1^+} \left(\frac{1}{(1/Sc) + (\varepsilon_D/\nu)} - \frac{1}{1 + (\varepsilon/\nu)} \right) dy^+. \tag{10}$$

The upper limit y_1^+ is an arbitrary value, large

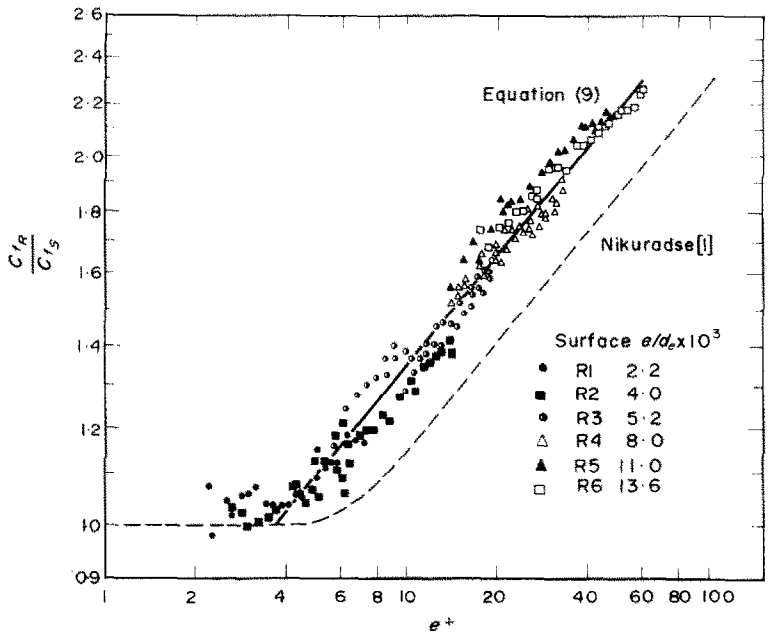

FIG. 15. Friction factor ratio vs. e^+, surfaces R1–R6.

enough to be outside the region where molecular properties are important.

The "law of the wall", which has been shown by Nikuradse to be valid for rough surfaces, gives

$$\frac{\varepsilon}{\nu} = fn(y^+, e^+). \tag{11a}$$

Similarly,

$$\frac{\varepsilon_D}{\nu} = fn(y^+, e^+, Sc). \tag{11b}$$

Thus, equation (10) becomes

$$\frac{\sqrt{(C_f/2)}}{St} - \frac{1}{\sqrt{(C_f/2)}} + F = g'(e^+, Sc). \tag{12}$$

The constant F, the fully rough value of $f(e^+)$, has been added to both sides of the equation to make the function g' consistent with Dipprey's g for heat transfer.

For high Schmidt numbers, the expression for g' can be simplified to

$$g'(e^+, Sc) = \frac{\sqrt{(C_f/2)}}{St} \tag{13}$$

as the other terms are small. Furthermore, applying equation (9), the similarity hypothesis reduces to

$$\frac{St_R}{St_S} = g''(e^+, Sc). \tag{14}$$

Thus, for any given Schmidt number, a plot of the Stanton number ratio against e^+ for the series of geometrically similar surfaces should yield a single curve.

The mass transfer data for surfaces R1–R6 have been plotted in this form in Figs. 16–18, using values of e^+ calculated iteratively from equation (9). The value of the friction factor ratio, C_{fR}/C_{fS}, from Fig. 15 is also plotted for comparison. The data are well correlated in this form for $e^+ > 25$, but as e^+ is decreased below 25, the curves for each roughness begin to deviate from the others in a positive direction, in the order of decreasing roughness size. In all cases, the point of deviation corresponds to a Reynolds number of roughly 15000–20000.

These deviations may result from inaccuracies in the data plotted. The probable random error

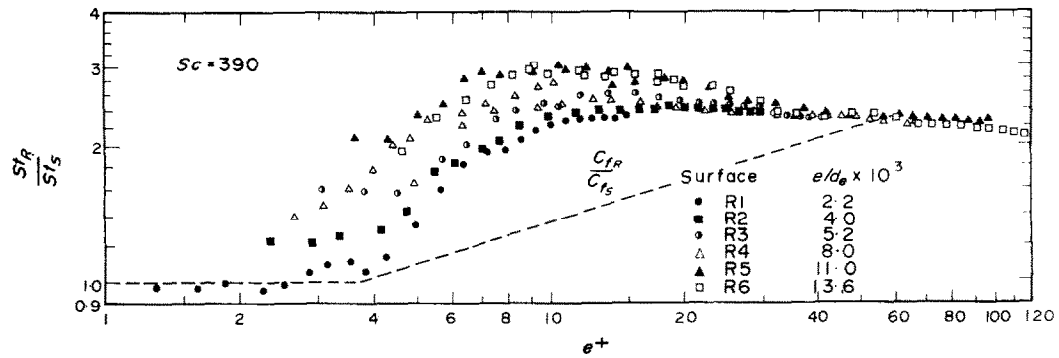

FIG. 16. Stanton number ratio vs. e^+, surfaces R1–R6.
$Sc = 390$

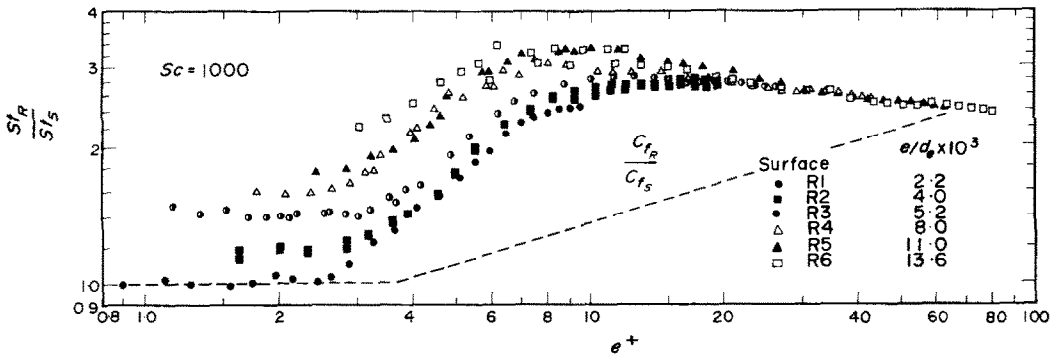

FIG. 17. Stanton number ratio vs. e^+, surfaces R1–R6.
$Sc = 1000$

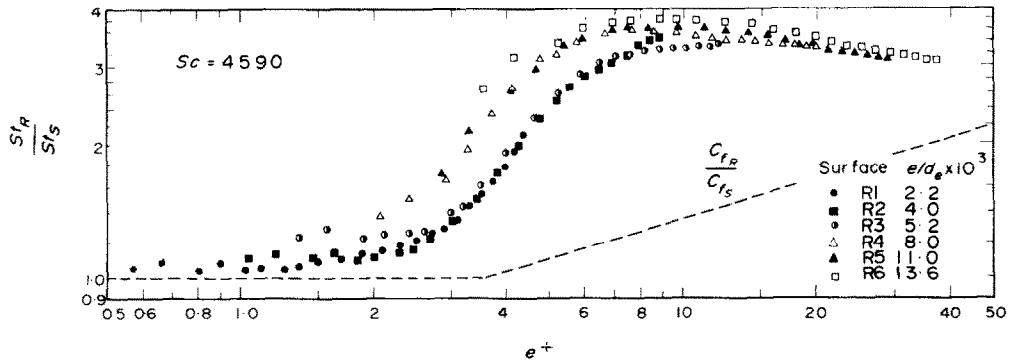

FIG. 18. Stanton number ratio vs. e^+, surfaces R1–R6,
$Sc = 4590$.

in the values of St and e^+ is estimated at 6 and 8 per cent respectively, at an average value of Re. In addition to the random error, however, systematic errors may also have resulted from assumptions made in the calculations.

One possible source of such an error in the Stanton number ratio is the assumption that entrance effects on the rough and smooth surface transfer coefficients will cancel. If this assumption is incorrect, its effect will be greatest at low Reynolds numbers. The use of equation (9) in the correlation introduces two possible sources of systematic error: several assumptions are inherent in the initial calculation and subsequent correction of the friction factor data, and the derivation of the form of equation (9) involves some approximations.

The deviations from similarity may of course also result from limitations in the similarity laws themselves. Dipprey [15] has pointed out that the similarity laws should not be expected to apply at low Reynolds numbers, since the "law of the wall" on which they are based is invalid in the region where the boundary layer occupies a significant portion of the pipe radius. It can be shown [11] that at $Re = 15000$, the effect of molecular properties extends to about 7 per cent of the pipe radius, not an unreasonable point to expect deviations to become noticeable.

Although significant deviations from similarity do occur at Reynolds numbers below about 15000, the data at higher Reynolds numbers do exhibit similarity, and the correlation can be used as a basis for discussion of the effect of roughness. The following discussion will be limited to those results which do exhibit similarity.

The hydraulically smooth region, $e^+ < 3$

Unfortunately, most of the data obtained for $e^+ < 3$ lie in the region where significant deviations from similarity occur. In fact, only surface R1 has a small enough roughness to escape this limitation. The similarity function plots for this surface however, can be considered representative of any similar roughness of smaller size ($e/d_e \leqslant 2{\cdot}2 \times 10^{-3}$)

For these small values of e/d_e, it is quite apparent that the roughness has little or no effect on the mass transfer rate in the hydraulically smooth region, in spite of the fact that the roughness height is greater than the thickness of the concentration boundary layer, i.e. the region in which most of the resistance to mass transfer occurs. Evidently the roughness, when submerged in the viscous sublayer, is not capable of generating sufficient turbulence to disrupt the concentration boundary layer.

This conclusion would indicate that the discrepancies in the literature data plotted in Fig. 1 cannot be attributed, as Brennan [3] has suggested, to the presence of minute roughnesses which are smaller than the viscous sublayer thickness.

This disparity may be partly resolved when one realizes that Brennan's data were obtained for an irregular, random roughness of the type which appears in dissolution studies. His roughnesses were reported as arithmetic average values obtained with a Brush surface analyser and extended up to 400 μin. Converting average values to peak-to-valley heights for a triangular shape would increase the numbers fourfold. Furthermore, it appears that random roughnesses give somewhat lower readings than regular, two-dimensional shapes, since some high peaks, or deep valleys, may go undetected. Making these allowances, Brennan's e^+ values range up to somewhere between $e^+ = 2$–3, close to the outer edge of the viscous sublayer. Also, one cannot exclude the possibility that the results of this paper, based on regular roughness elements do not apply to surfaces with random roughness. The disparity, therefore, is likely not as serious as it would appear at first sight.

The transition region, $3 < e^+ < 25$

The transition region is characterized by a marked increase in the transfer coefficient over the approximate range $3 < e^+ < 10$. By comparing the data with the friction factor curve on

the same graph, it can be seen that the increase in the mass transfer rate is much greater than in the friction factor over this range. Transition begins at about the same e^+ for both St and C_f; above $e^+ \sim 10$, however, the Stanton number ratio levels off, while the friction factor ratio continues to rise.

The transition region can be considered as the region in which the roughness emerges from a previously unaffected viscous sublayer. It is not necessary, however, to assume that the sublayer has not been changed by the presence of a submerged roughness. Perhaps a more acceptable description of the flow near the roughness elements is that shown in Fig. 19.

Consider the viscous sublayer to grow on the roughness element; the sublayer will be thicker between the roughnesses, and quite thin at the peaks. As Re is increased, the sublayer will decrease in thickness. Eventually the thin layer at the peak will be disrupted, and the turbulence generated will be transmitted into the valleys between the roughness elements. As Re is further increased, the valley regions will become more turbulent until, in the fully rough region, only a thin sublayer will remain.

These changes in the turbulence level near the rough surface would have an effect on both the momentum and mass transfer rates. Disruption of the viscous sublayer and penetration of turbulence into the valley regions would result in rapid increases in the rates of both momentum and mass transfer. A greater increase in the latter would be expected, as proportionately more of the resistance to mass transfer occurs in the viscous region.

The levelling off of the Stanton number ratio above $e^+ \sim 10$, unlike the friction factor ratio, is not inconsistent with the assumption of an analogy between the transfer processes. Since ε/ν and ε_D/ν, and therefore g', are functions of e^+, the analogy as expressed by equation (12) does not require that the dependence of these ratios on e^+ or on Re be the same.

The Schmidt number apparently influences the similarity plots in two ways; at higher Sc, not only is the increase in the transfer greater, but it also occurs at lower values of e^+. Since the low rate of molecular diffusion very near the wall is the major resistance to transfer, any turbulence which reaches the wall would be expected to cause a greater increase in mass transfer rates in lower diffusivity, or higher Schmidt number, systems. The apparent shift of the transition region to lower values of e^+ at high Schmidt numbers is probably just a reflection of the greater influence of a given level of turbulence.

The fully rough region, $e^+ > 25$

In the region $e^+ > 25$, the similarity function provides a good correlation of the results for all the geometrically similar surfaces. A linear plot is obtained for each Schmidt number, having a small negative slope.

A least-squares correlation of the data points for $e^+ > 25$ yielded the equation

$$\frac{St_R}{St_S} = 1{\cdot}94\, Sc^{0{\cdot}09}\, e^{+-0{\cdot}10};\ 25 \leqslant e^+ \leqslant 120 \quad (15)$$

with a standard deviation of 3·3 per cent. This equation, combined with the smooth surface correlation, equation (6), is sufficient to

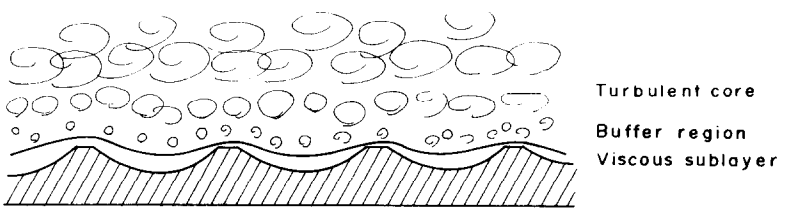

FIG. 19. Suggested flow pattern near the rough wall.

describe the mass transfer results for the geometrically similar roughnesses in the fully rough region.

The success of this method of correlation for $e^+ > 25$ indicates that an analogy does exist between the processes of momentum and mass transfer, as the similarity functions are based on this assumption. The existence of such an analogy, however, does not change a conclusion drawn earlier: the friction factor alone is not sufficient to correlate mass transfer results from different rough surfaces. The function g' is the most general expression of the analogy. For smooth surfaces, g' is a function only of Sc, and it is therefore possible to correlate St with C_f. For rough surfaces, however, g' is also dependent on e^+; thus St can be correlated with C_f only when a common relationship exists between C_f and e^+, i.e. only for geometrically similar roughnesses.

A comparison of the present mass transfer data can be made with the heat transfer results of Dipprey [2], using the similarity functions g' and g. Combining equations (15) and (9) with the definition of g', equation (13), yields

$$g'(e^+, Sc) = 5{\cdot}5\, e^{+0{\cdot}25}\, Sc^{0{\cdot}58};\ 25 \leqslant e \leqslant 120. \quad (16)$$

Dipprey's equivalent equation for heat transfer is

$$g(e^+, Pr) = 5{\cdot}19\, e^{+0{\cdot}20}\, Pr^{0{\cdot}44}. \quad (17)$$

Most heat transfer studies [2, 4] have shown that $St \propto Re^{-0{\cdot}2}$, or equivalently $g \propto e^{+0{\cdot}2}$, for a variety of roughness shapes. The exponent of 0·25 determined in the present work is in reasonable agreement, particularly considering the lack of precision in the friction factor measurements, and the narrow range of e^+ over which these data were obtained.

The difference in the exponents on Sc and Pr is not unexpected, as Dipprey's data were at low Prandtl number ($1{\cdot}2 \leqslant Pr \leqslant 6$). A similar trend is experienced with smooth surfaces, the exponent varying from 0·60 at low Sc or Pr, to 0·67 at $Sc > 100$. Gowen's rough surface heat transfer data [4] covered the range $0{\cdot}7 \leqslant Pr \leqslant 14$; an exponent of 0·51 was observed, intermediate between those of equations (16) and (17).

SUMMARY AND CONCLUSIONS

Mass transfer coefficients have been measured for a series of geometrically similar rough surfaces, using the electrochemical technique. The technique was found to be particularly suited to such a study, where it is important that the geometry of the surface be known and constant.

Friction factors for the series of roughnesses were adequately correlated by the friction similarity function, $f(e^+)$. A simpler correlation is obtained by plotting the ratio C_{f_R}/C_{f_S} against the dimensionless roughness height, e^+. The corresponding mass transfer similarity function, $g'(e^+, Sc)$ can be reduced to the ratio St_R/St_S in high Sc systems. This ratio correlated the data for the similar series well for Reynolds numbers greater than about 15000, illustrating that the processes of momentum and mass transfer near rough surfaces are analogous.

Significant deviations from similarity occurred at Reynolds numbers less than 15000, which may have resulted from inaccuracies in the data or limitations in the similarity laws. Surfaces having very small roughnesses ($e/d_e \leqslant 2{\cdot}2 \times 10^{-3}$), which are in the hydraulically smooth region at $Re > 15000$, yield mass transfer coefficients equal to those for smooth surfaces. Outside the hydraulically smooth region, roughness can increase the mass transfer rate by as much as a factor of four in high Sc systems. The greatest increases occur in the transition region.

ACKNOWLEDGEMENT

Financial assistance from the National Research Council of Canada is gratefully acknowledged. D. A. Dawson expresses his thanks to NRC for scholarship aid.

REFERENCES

1. J. NIKURADSE, Laws for flow in rough pipes, *V.D.I. Forsch.* **361B**, 4 (1933); NACA TM 1292 (1950).
2. D. F. DIPPREY and R. H. SABERSKY, Heat and momentum transfer in smooth and rough tubes at various Prandtl numbers, *Int. J. Heat Mass Transfer* **6**, 329–352 (1963).

3. W. C. BRENNAN, Mass transfer in turbulent pipe flow. The effect of surface roughness, M.A.Sc. Thesis, Dept. of Chemical Eng., University of Toronto (1963).
4. R. A. GOWEN, A study of forced convection heat transfer from smooth and rough surfaces, Ph.D. Thesis, Dept. of Chem. Eng., University of Toronto (1967).
5. C. S. LIN, R. W. MOULTON and G. L. PUTMAN, Mass transfer between solid wall and fluid streams, *Ind. Engng Chem.* **45**, 636–646 (1953).
6. W. E. RANZ, Electrolytic methods for measuring water velocities, *A.I.Ch.E. Jl* **4**, 338–342 (1958).
7. L. P. REISS and T. J. HANRATTY, Measurement of instantaneous rates of mass transfer to a small sink on a wall, *A.I.Ch.E. Jl* **8**, 245–247 (1962).
8. L. P. REISS and T. J. HANRATTY, An experimental study of the unsteady nature of the viscous sublayer, *A.I.Ch.E. Jl* **9**, 154–160 (1963).
9. P. V. SHAW, L. P. REISS and T. J. HANRATTY, Rates of turbulent transfer to a pipe wall in the mass transfer entry region, *A.I.Ch.E. Jl* **9**, 362–364 (1963).
10. J. S. SON and T. J. HANRATTY, Limiting relation for the eddy diffusivity close to a wall, *A.I.Ch.E. Jl* **13**, 689–696 (1967).
11. D. A. DAWSON, High Schmidt number mass transfer near rough surfaces, Ph.D. Thesis, Dept. of Chem. Eng., University of Toronto (1968).
12. D. W. HUBBARD and E. N. LIHHTFOOT, Correlation of heat and mass transfer data for high Schmidt and Reynolds numbers, *I/EC Fundamentals* **5**, 370–379 (1966).
13. P. HARRIOT and R. M. HAMILTON, Solid–liquid mass transfer in turbulent pipe flow, *Chem. Engng Sci.* **20**, 1073–1078 (1965).
14. T. K. SHERWOOD, Mass, heat, and momentum transfer between phases, *Chem. Engng Prog. Symp. Ser.* No. 25, **55**, 71–85 (1959).
15. D. F. DIPPREY, personal communication (1968).
16. E. S. C. MEYERINK and S. K. FRIEDLANDER, Diffusion and diffusion controlled reactions in fully developed turbulent pipe flow, *Chem. Engng Sci.* **17**, 121–135 (1962).
17. W. H. LINTON and T. K. SHERWOOD, Mass transfer from solid shapes to water in streamline and turbulent flow, *Chem. Engng Prog.* **46**, 258–264 (1950).
18. C. STIRBA and D. M. HURT, Turbulence in falling liquid films, *A.I.Ch.E. Jl.* **1**, 178–184 (1955).
19. M. K. KISHINEVSKY, T. B. DENISOVA and V. A. PARMENOV, The study of mass transfer from the wall of a smooth tube to a turbulent liquid flow at high Schmidt numbers, *Int. J. Heat. Mass Transfer* **9**, 1449–1453 (1966).

TRANSFERT MASSIQUE AUX SURFACES RUGUEUSES

Résumé—Des flux de transfert massique électrochimique entre des surfaces solides de nickel et l'électrolyte ferro-ferricyanure s'écoulant dans un conduit à section carrée de 2,54 cm de côté, ont été mesurés pour une surface lisse et six surfaces rugueuses semblables, ces dernières ayant des sillons en V de 5.10^{-2} mm à 0.36 mm de profondeur et perpendiculaires à la direction de l'écoulement. Le nombre de Reynolds varie de 3 000 à 120 000 et le nombre de Schmidt de 300 à 4 600.

Pour les nombres de Reynolds supérieurs à 15 000 environ, les résultats sont représentés par

$$\frac{St_R}{St_s} = \frac{k_R}{k_s} = f(e^+, Sc)$$

Un effet maximal de la rugosité a été observé à la hauteur réduite de rugosité $e^+ = 10$ où le rapport du transfert pour la surface rugueuse à celui relatif à la surface lisse varie entre 3 et 4.

Des essais pour des surfaces dissemblables montrent l'importance de la forme et du pas des rugosités; leur influence sur le transfert massique est différente de celle sur le transfert de quantité de mouvement.

STOFFTRANSPORT AN RAUHEN OBERFLÄCHEN

Zusammenfassung—Es wurde der elektrochemische Stofftransport zwischen festen Nickeloberflächen und einem Ferro-Eisenzyanidelektrolyten in einem quadratischen Kanal von 25.4 mm Seitenlänge gemessen.

Angeströmt wurden sechs rauhe Oberflächen mit V-förmigen Rillen quer zur Strömungsrichtung, von 0.05–0.35 mm Tiefe, und eine glatte Oberfläche. Die Reynoldszahlen wurden zwischen 3000 und 120 000, die Schmidtzahlen zwischen 390 und 4600 variiert. Für Reynoldszahlen, die grösser waren als 15 000 konnte folgende Beziehung aufgestellt werden

$$\frac{St_R}{St_S} = \frac{k_R}{k_S} = f(e^+, Sc).$$

Ein maximaler Rauhigkeitseffekt wurde bei der dimensionslosen Rauhigkeitshöhe $e^+ \approx 10$ beobachtet, wobei der Stofftransport an rauhen Oberflächen 3 bis 4 mal grösser als an der glatten Overfläche war.

Die Ergebnisse an verschiedenen Oberflächen zeigten die Bedeutung von Gestalt und Grösse der Rauhigkeit. Dieser Einfluss auf den Stofftransport ist vom Impulstransport zu unterscheiden.

ПЕРЕНОС МАССЫ НА ШЕРОХОВАТЫХ ПОВЕРХНОСТЯХ

Аннотация—Электрохимическим методом измерялись потоки массы между твердыми никелевыми поверхностями и ферро-ферри-цианидным электролитом, текущем в трубе квадратного поперечного сечения со стороной в 1 дюйм. Измерения проводились в гладких и шероховатых трубах. Шероховатые трубы имели V-образные канавки глубиной от 2 до 14 миллиметров, расположенные перпендикулярно направлению течения. Число Рейнольдса изменялось от 3 000 до 120 000, а число Шмидта—от 390 до 4 600.

Для значений числа Рейнольдса, превышающих 15 000, эти данные коррелируются следующим образом:

$$\frac{St_R}{St_S} = \frac{k_R}{k_S} = f(e^+, Sc)$$

Максимум влияния шероховатости наблюдался при безразмерной высоте шероховатости $e^+ \simeq 10$, когда отношение переноса массы на шероховатой поверхности к переносу массы на гладкой поверхности изменялось от 3 до 4. Данные для различных шероховатых поверхностей указывают на существенность формы шероховатости и ее шага; их влияние на перенос массы отличается от влияния на перенос количества движения.